



## **Pulse plating as an alternative approach to improve Ni-Co alloys properties coated from a bath with a low nickel content**

**I. Kharmachi <sup>a,b</sup>, L. Dhouibi <sup>a</sup>, P. Berçot <sup>b</sup>, M. Rezrazi <sup>b</sup>**

<sup>a</sup> *Unité de recherche Mécanique-Energétique, Equipe Corrosion et Protection des Métalliques, ENIT, Université de Tunis El-Manar, BP 37, Tunis Belvédère, 1002, Tunisia*

<sup>b</sup> *Institut UTINAM, CNRS UMR 6213, Université de Franche-Comté, 16 route de Gray, 25030 Besançon Cedex, France*

Received 16 Sep 2015, Revised 23 Feb 2016, Accepted 08 Mar 2016

\*For correspondence: Email: [imen.kharmachi@univ-fcomte.fr](mailto:imen.kharmachi@univ-fcomte.fr) (I.Kharmachi); Phone: (+21696477524)

### **Abstract**

The effect of pulse plating on the properties of Ni-Co alloys was presented in this paper especially on the surface morphology, microstructure, composition and crystal size. The analytical characterization of Ni-Co coating was investigated by scanning electron spectroscopy (SEM), X-ray diffraction (XRD) and GDOES analyses. The corrosion performance of Ni-Co alloy coatings were evaluated in 3% NaCl solution by means of potentiodynamic polarization. The results showed that the deposits morphology was quite different; it changed from irregular deposit with imperfections obtained by continuous currents (cc), to smooth and regular surface with an average of grain size about 6 nm for the deposit obtained by pulsed currents (pc). The electrochemical results revealed that the protection of carbon steel substrate against corrosion was better with Ni-Co alloys obtained by the pulse electrodeposition mode than by the continuous currents coated from the same bath composition. Furthermore, an improvement in corrosion resistance and a high quality of Ni-Co coatings were detected with low content of nickel in the bath which could reduce toxicity and with using pulse-plating mode than other deposits produced by continuous currents with high nickel amounts.

*Keywords:* Ni-Co alloys, electrodeposition, nickel amount, continuous currents (cc), corrosion, pulsed currents (pc).

### **1. Introduction**

The use of electroplating technique to produce coatings is a most interesting method due to the possibility of deposition as single layer or multi-layer coatings on planar and non-planar substrates, the efficiency, the low cost and the ease of high volume production, in contrast with other techniques such as sputtering and chemical vapor deposition [1,2].

Up to now, nickel electroplating is exploited in large number of industrial applications due to each properties [3,4]. Compared to pure nickel, Ni-Co alloy possesses much advantages; good adhesion and wear resistance, better hardness, corrosion resistance, heat conductive and excellent magnetic properties [5-8]. As these alloys are known as good magnetic materials since 1921 [9,10], the Co-Ni alloy thin films are used in various magnetic devices, especially in micro system technology for manufacture of sensors, actuators and memory devices [11,12]. These properties of Ni-Co alloys are affected by many electroplating parameters; in particular the composition of the electroplating bath which represented with Ni/Co ratio. Several researchers develop coatings with high Ni/Co ratio [13,14] which means the introducing of large amounts of nickel in the electroplating electrolyte.

Recent updates concern nickel metal and its salts which have generated environmental concerns and health hazards and have been classified as CMR. Environmental constraints lead to increasingly severe regulation. Nickel is a carcinogenic metal known to be an environmental and occupational pollutant [15]. It has been identified as a toxin that severely damages reproductive health and can lead to infertility. Thus, alternatives should be used in order to reduce nickel amount in the plating bath and produce in parallel high quality coatings.

In the recent years, compared to continuous current, pulse current plating has received a considerable attention as an economically processing technique of deposition. The quality of coating was better by pulse electrodeposition than direct current. It has been shown that pulse current deposition is able to produce coatings

with excellent properties in morphology, particle distribution, structure, grain size, hardness and wear resistance [16-18].

The pulse plating was a technique identified to lower stress, to change the morphology, composition, microstructure and to enhance deposit properties [19]. The predominant feature in electrodeposition by pulsed current is the possibility of using high instantaneous current densities which in continuous current plating lead generally to rough and powdery deposits [20]. Some studies were carried out on the pulse plating of Ni-Co alloys. Tury et al. [21] elucidated the effect of the variation of pulse parameters on the composition, morphology and structure of Ni-Co alloys electrodeposited from a chloride bath. Yundong et al. [13] found that the variation of the peak current density has significant impact on the microstructure, finer grain size, microhardness and tensile strength of nanocrystalline Ni-Co alloy deposit produced by pulse plating method and J. Vazquez-Arenas et al. [22,23] studied whether the use of pulse or pulse reverse plating can overcome the anomalous behavior of this system whereby cobalt preferentially deposits over nickel even from solutions containing more NiSO<sub>4</sub> than CoSO<sub>4</sub> and proved that the anomalous behavior of Co-Ni deposition could be alleviated through use of cyclic voltammetry or pulse reverse plating and deposition is less anomalous when the electroplating bath is quiescent.

Thus, the main objective of the current study is to use pulse electrodeposition technique as alternative approach in order to reduce nickel concentration in the sulfate plating media and achieve high quality of Ni-Co coating and a better corrosion resistance similar to deposits obtained by continuous currents from plating solution containing large amounts of nickel.

## 2. Materials and methods

### 2.1. Electroplating conditions

The composition of plating bath of Ni-Co alloys deposition was shown in Table 1. The pulse and the continuous electrodeposition process of Ni-Co coatings were carried out at room temperature, on carbon steel substrate and after immersion of 30 min in the sulfate media.

A low carbon steel panel with plated area of 0.2 cm<sup>2</sup> was used to perform galvanostatic measurements. The chemical composition of the steel cathode (STUB 100CR6) was 0.45% C, 1.5% Mn, 0.45% Si and 0.06% S (wt.%). The steel substrates were polished with SiC grinding paper (SiC #320, #600, #800, #1200, #2400) cleaned with acetone using ultrasonics-cleaning equipment for 2 min, and then rinsed with distilled water and dried.

**Table 1:** Electrolyte composition and deposition conditions for Ni-Co binary coatings.

Bath composition	Concentration (g L <sup>-1</sup> )	Plating Parameters	$R = \frac{[Ni^{2+}]}{[Co^{2+}]}$ in bath
NiSO <sub>4</sub> .6H <sub>2</sub> O	[6, 300]	Temperature: 25±2°C	[1, 50]
CoSO <sub>4</sub> .7H <sub>2</sub> O	6		
H <sub>3</sub> BO <sub>3</sub>	40		
Saccharin	3		

### 2.2. Electrochemical measurements

A 3-electrode cell was used to conduct the electrochemical experiments. The counter electrode was platinum with an area of 1 cm<sup>2</sup> and the carbon steel as working electrode. For electrodeposition process, the Saturated Sulfate Reference electrode (SSE) was used to prevent presence of chloride ions in sulfate bath. However, for the corrosion test in 3% NaCl solution, reference electrode was the Saturated Calomel Electrode (SCE).

The coated sample was exposed to 3 % NaCl media and potentiodynamic polarization curves were used to study the corrosion behavior of Ni-Co alloy coatings. These potentiodynamic measurements were obtained by means of a potentiostat-galvanostat Radiometer Copenhagen PGZ 402 model, piloted by Voltlab4 software.

The measurements were performed at room temperature, the sample was immersed in the corrosive medium for 1 hour to attain open circuit potential (E<sub>ocp</sub>) or the steady state potential. After the stabilization of the open circuit potential, the upper and the lower potential limits were fixed to ±250 mV with respect to E<sub>ocp</sub> in order to determine the polarization resistance values using Tafel plot. The polarization curves were a linear scan from E<sub>1</sub> cathodic potential (-1000 mV/SCE) to E<sub>2</sub> anodic potential (100 mV/SCE) using a scan rate of 0.5 mV/s.

### 2.3. Characterization studies

Scanning electron microscopy (SEM) was carried out using a JEOL type 5600 associated to an energy dispersive spectroscopy (EDS) FONDIS model to determine the approximate composition of the alloy.

The crystal orientation was determined using an X-ray diffractometer D8 (Advance Bruker) equipped with a copper anode generating Ni-filtered employing CuK $\alpha$  radiation of wavelength 0.154 nm. The crystallite size of Co–Ni coating was determined, applying line broadening technique using Scherrer equation Eq. (1) [24]:

$$D = \frac{K\lambda}{\beta \cos \theta} \quad (1)$$

Where K is the Scherrer factor  $\approx 1$ , D is the crystallite size,  $\lambda$  is the incident radiation wavelength,  $\beta$  is the integral breadth of the structurally broadened profile and  $\theta$  is the angular position.

The metals existing in the deposit were detected by depth profiling using Glow Discharge Optical Emission Spectroscopy (GDOES) type Jobin Yvon GD Profiler instrument equipped with a 4 mm diameter anode and operating after optimization at a pressure of 650 Pa and a power of 30 W in an argon atmosphere. This low power was retained to decrease the speed of abrasion of the deposits with low thickness and to obtain maximum information at the surface.

Quantified compositional results were evaluated automatically utilizing the standard Jobin Yvon quantum Intelligent Quantification software. The instrument was calibrated with standard with known composition. Depths were calculated using relative sputter rates, obtained from the sputter yields of each major element with corrections for composition and discharge conditions.

Measurements of the Vickers microhardness (HV) of deposits were performed on the surface by using a HMV-M3 SHIMADZU microhardness tester under 25 g to 100 g load for 10 s and the corresponding final values were determined as the average of 5 measurements.

## 3. Results and discussion

### 3.1. Ni-Co coatings electrodeposited from high nickel electrolyte using continuous-plating mode

#### 3.1.1 Optimization

The pH of the electroplating bath, current density and atomic ratio  $R = \frac{[Ni^{2+}]}{[Co^{2+}]}$  in the electrolyte are considered to be the most important factors to synthesize a resistant layer against chloride ions and to make the electrodeposition in best conditions (Table 2).

A Doehlert design, with 13 experiments for 3 factors, was carried out as a screening approach to optimize those experimental conditions using NEMROD software program (L.P.R.A.I, Marseille, France) (Table 2). The polarization resistance Rp, determined from the potentiodynamic polarization curves, was exploited as response of Ni-Co deposits recorded in 3% NaCl.

Mathematical approach for the responses equation:

$$Y = 740,0 - 43,1 X_1 - 374,3 X_2 + 777,7 X_3 - 321,5 X_1^2 + 367,1 X_2^2 + 626,0 X_3^2 + 184,7 X_1 X_2 - 156 X_1 X_3 - 698,4 X_2 X_3$$

X<sub>1</sub>: pH of the electroplating bath

X<sub>2</sub>: I (mA cm<sup>-2</sup>) current density

X<sub>3</sub>: atomic ratio  $R = \frac{[Ni^{2+}]}{[Co^{2+}]}$  in bath

Y: Rp ( $\Omega$  cm<sup>2</sup>) the polarization resistance of Ni-Co coatings

**Table 2:** A table summarizing the different factors and optima conditions.

		X <sub>i</sub> : factors		
		X <sub>1</sub> = pH	X <sub>2</sub> = I (mA cm <sup>-2</sup> )	X <sub>3</sub> = R
Experimental field	Low limit (-)	1	25	1
	Upper limit (+)	5	50	50
Optima conditions	X <sub>i</sub> optimum	2	25	50

Fig. 1-A, B and C translate the evolution of Rp with the interaction between pH, I and R. The examination of this figure shows that optima conditions relative to the highest Rp values are R=50, pH=2 and I=25 mA cm<sup>-2</sup> for electrodeposition with continuous currents (cc).

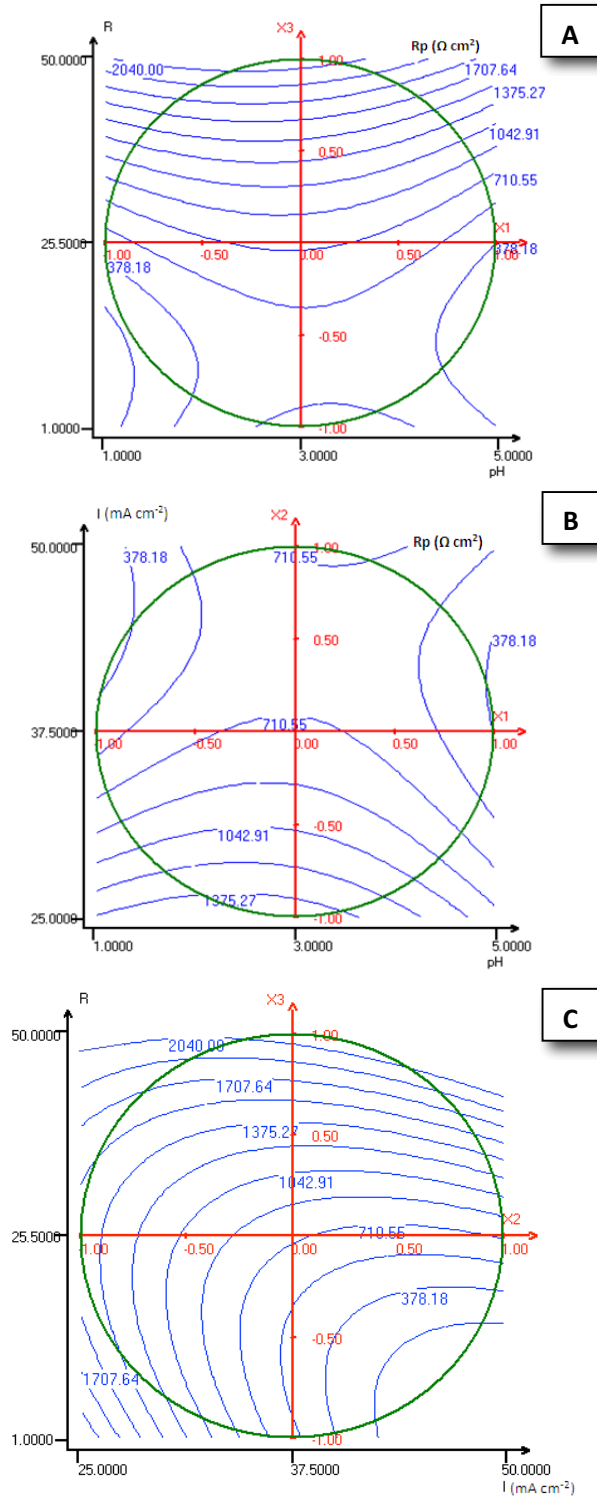


**Fig. 1.** Isoresponse curves for the modeling polarization resistance  $R_p$  ( $\Omega \text{ cm}^2$ ) of Ni-Co coatings on carbon steel substrate function of pH, I (current density) and the atomic ratio  $R = \frac{[Ni^{2+}]}{[Co^{2+}]}$  in the electroplating bath.

### 3.1.2 Electroplating and film Characterization

The continuous electrodeposition process was carried out in optima conditions ( $I=25 \text{ mA cm}^{-2}$ ,  $R=50$ ,  $\text{pH} = 2 \pm 0.2$ ). Fig. 2 shows the potential-time evolution in the electrodeposition of nickel-cobalt alloy on carbon steel substrate for 30 min. Since the immersion, the potential falls instantly to  $-1100 \text{ mV/SSE}$  and the deposition takes place with low nucleation overpotential (part A in the curve).

According to the literature [25], this potential drop is due to the charge of the double layer at the interface electrode-electrolyte, which shows the charge transfer of ions  $\text{Ni}^{2+}$  and  $\text{Co}^{2+}$  made at the beginning of electrodeposition process. In the second part B, the potential is ennobled quickly which indicates the presence of an adsorption phenomenon of atoms Ni or Co, then the electrodeposition potential becomes stable at a higher value -1040 mV/SSE. Which corresponds to the phase of germination or nucleation in the deposition process and the potential stability is related to the crystal growth (part C in the curve).

Liangliang et al. [26] suggested that after being reduced from metal ions to metal atoms in the electrolyte, these metal atoms were adsorbed on the surface of the cathode and stable crystal nuclei were formed by the aggregation of many germs. This phenomenon was known as electrocrystallization process that was characterized by the formation of two dimensional crystal nuclei.

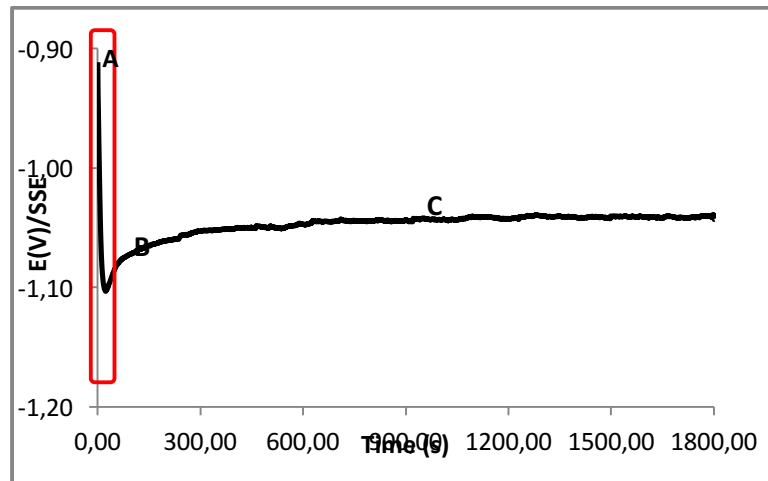


**Fig. 2.** Deposition potential-time of Ni-Co alloy on carbon steel substrate, under optima conditions ( $I=25 \text{ mA cm}^{-2}$ ,  $\text{pH}=2$ ,  $R=50$ ).

Fig. 3 illustrates the SEM image of the surface morphology of Ni-Co film deposited on carbon steel substrate in optima conditions. A smooth surface is observed with little irregularity. The EDS analysis indicates that the Co content is about 9% in the deposit.

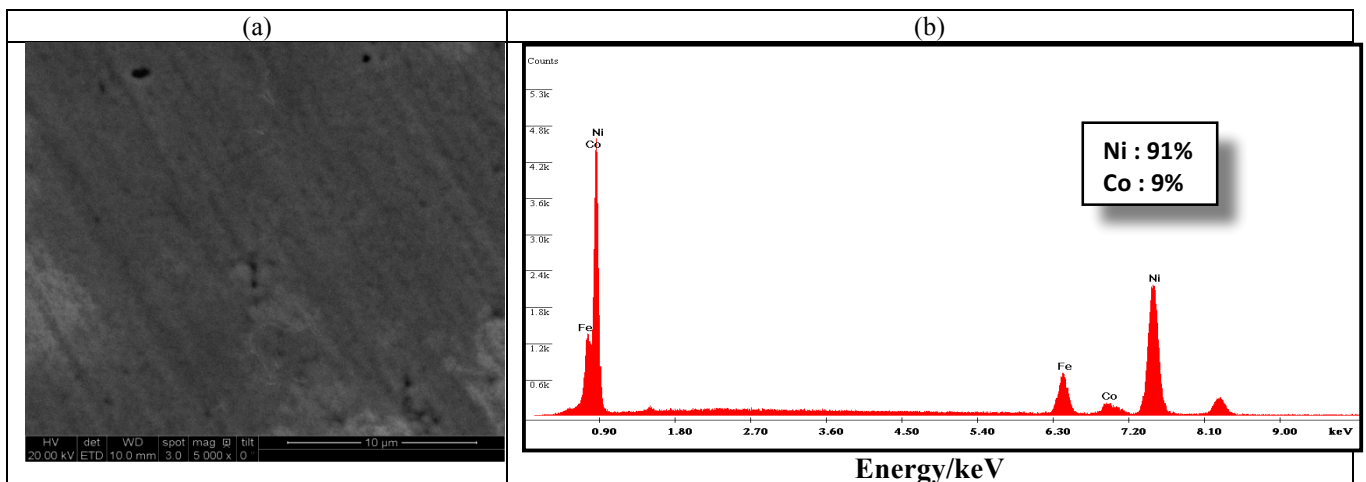


**Fig. 3.** SEM image (a) and Energy Dispersive Spectroscopy EDS spectra (b) of Ni-Co coated steel in optima conditions ( $I=25 \text{ mA cm}^{-2}$ ,  $\text{pH}=2$ ,  $R=50$ ).

Fig. 4 depicts the GDOES depth profile of the same deposit, which indicates the percentage of different selected species (nickel, cobalt and iron) that can be exist in the deposit. The distribution of the different metals is disclosed clearly with sharply defined interface between the film and the substrate. The Glow Discharge Optical Emission Spectroscopy (GDOES) is based on the sputtering process and different depths can be eroded.

The nickel and cobalt metals are uniformly dispersed inside the deposit and the substrate is appeared after an erosion of a depth about 5 $\mu\text{m}$  which probably corresponds to the thickness of electrodeposited film. The Co amount in the deposit is about 9% which is confirmed by EDS analysis.

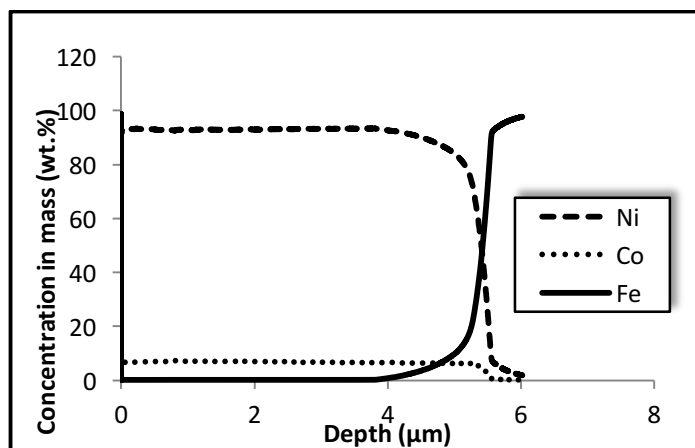


Fig. 4. GDOES depth quantified profile of Ni-Co alloy coatings electrodeposited in optima conditions ( $I=25 \text{ mA cm}^{-2}$ ,  $\text{pH}=2$ ,  $R=50$ ).

Fig. 5 presents the XRD patterns of Ni-Co coating (Ni-9wt.% Co) deposited on carbon steel substrate under optima conditions in continuous currents. The binary Ni-Co phase diagram [27] indicates that the structure consists of  $\alpha$  phase, which is a substitutional solid solution of Ni and Co and the structure was face centered cubic (fcc). In this study, the fcc peaks are observed in XRD result of Ni-Co coating pattern. Three peaks with the orientation (111), (200) and (220) are appeared respectively for 2 Theta  $\approx 44^\circ$ ,  $52^\circ$  and  $76^\circ$  corresponding to different crystal faces with the predominance of (111) orientation which matches well with the standard Ni-Co structure.

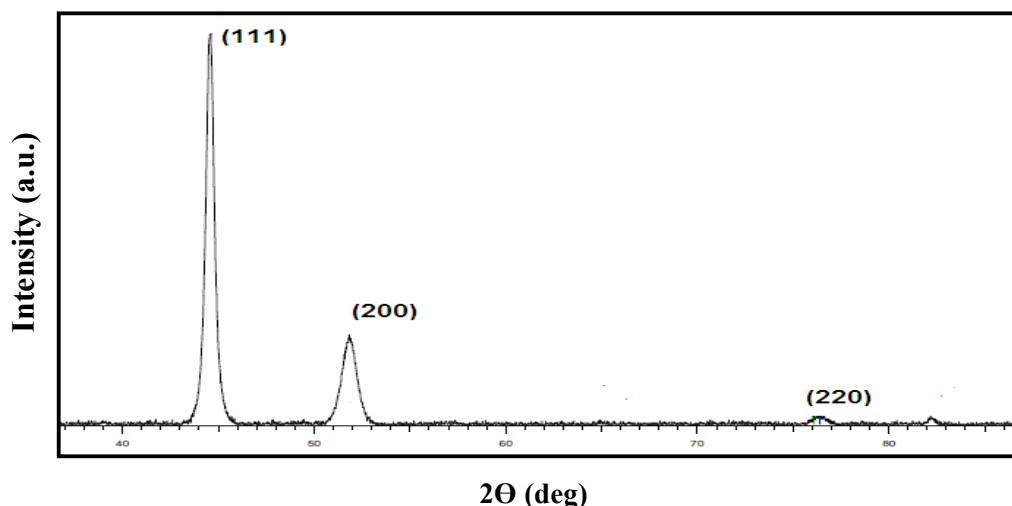


Fig. 5. X-ray diffraction pattern of Ni-Co binary coatings deposited from the electrolyte ( $I=25 \text{ mA cm}^{-2}$ ,  $\text{pH}=2$ ,  $R=50$ ).

The Ni-Co coatings electrodeposited under previous conditions revealed a smooth and uniform morphology with a thickness about 5  $\mu\text{m}$ . But, a large amount of nickel ( $300 \text{ g L}^{-1}$ ) was introduced in plating bath during the electrodeposition process and the Ni content in the deposit was about of 91%.

Since 2010, nickel salts have been classified as CMR, they have generated environmental problems and many health hazards [15]. So, we find that is interesting to reduce nickel amount in the sulfate plating bath from  $300 \text{ g L}^{-1}$  to  $60 \text{ g L}^{-1}$  (from  $R=50$  to 10) in order to reach Ni-Co alloys properties comparable to electroplating bath ( $R=50$ ) using pulse electrodeposition process.

### 3.2. Comparative study of the physicochemical properties of continuous current-plated and pulse-plated Ni-Co alloys from low nickel plating bath

The electrodeposition of Ni-Co alloys in continuous currents (cc) and pulsed currents (pc) was carried out at room temperature and after immersion of 30 min in less nickel sulfate media ( $I=25 \text{ mA cm}^{-2}$ ,  $\text{pH}=2 \pm 0.2$ ,  $R=10$ ).

#### 3.2.1. Conditions of pulse electrodeposition

In this part, we kept the same charge quantities as continuous currents [28]. The pulsed parameters calculated were:

$$t_{\text{on}}=1 \text{ ms}, t_{\text{off}}=79 \text{ ms and } I_c = -2.10^3 \text{ mA cm}^{-2}$$

In the pulsed electrodeposition, there are three important parameters affecting the coating properties; the time period that the pulses are imposed (on-time,  $T_{\text{on}}$ ), the relaxation time (off-time,  $T_{\text{off}}$ ), the cathodic current density  $I_c$  and the average current density ( $I_m$ ) that's equivalent to the current density ( $I=25 \text{ mA cm}^{-2}$ ) applied in the continuous electrodeposition process Eq. (2) [28]:

$$I_m = I_c \frac{T_{\text{on}}}{T_{\text{on}}+T_{\text{off}}} = I_c T_{\text{on}} \nu = \alpha I_c \quad (2)$$

Where  $\nu$  is the pulse frequency and  $\alpha$  the duty cycle.

#### 3.2.2. Composition, anomalous behavior and surface morphology of Ni-Co alloys

The SEM images of the coated carbon steel samples (Fig. 6) show that Ni-Co coating obtained by continuous current (cc) was gray, shining and presents zones of irregularity with big grains, whereas the pulsed electrodeposit presents a different granulated morphology with well-defined grains, about 6 nm in size which cover the totality of the surface. The EDS patterns of Ni-Co coatings are shown in Fig. 8. Layer obtained by (cc) contains 24% of cobalt. However, the layer obtained by (pc) contains 34%. The Co content in the deposit increased which was confirmed by XRF analysis.

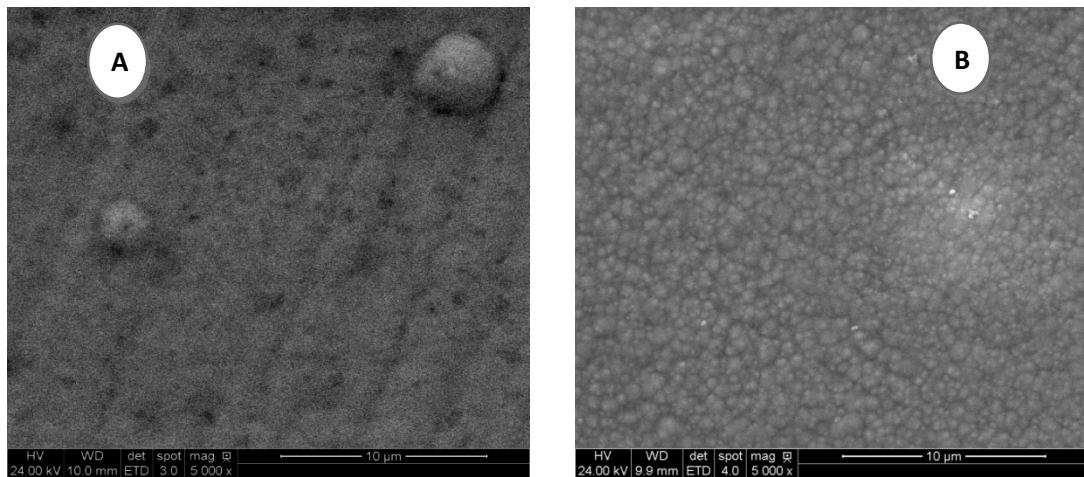


**Fig. 6.** SEM images of Ni-Co alloys  $R=10$  obtained by (a): continuous and (b): pulsed currents

The X-ray fluorescence results are presented in Table 3. As shown in the table, the cobalt content in deposit increased from 25 wt.% in continuous current (cc) to 36 wt.% with (pc) method and microhardness of alloy increased from 350 HV to 392 HV. The Co content of the film was depending on the percentage of cobalt in electrolyte. The percentage of Co in the film was higher than the percentage in the electrolyte [29]. Several studies have been put in literature to understand the phenomenon. This refers to anomalous behavior of nickel and cobalt ions that was studied by Brenner [30]. He has explained anomalous codeposition of binary alloys of the iron group metals as the member that shows retardation of discharge in codeposition is the one that normally deposits with the higher over voltage. Some researchers have proposed electrodeposition mechanism which characterized by the rise of pH at the cathode.

**Table 3:** A summary of composition analysis, thickness, hardness and grain size for Ni-Co deposits in (cc) and (pc).

Deposit	XRF analysis ( $\pm 0.2$ wt.%)		Thickness ( $\pm 0.1 \mu\text{m}$ )	Microhardness ( $\pm 5$ HV)	Grain size ( $\pm 0.1$ nm)
	Co (wt.%)	Ni (wt.%)			
Ni-Co in cc (R=10)	25	75	5	350	8.2
Ni-Co in pc (R=10)	36	64	2.5	392	6.5

This local increase in pH caused by the precipitation of metal hydroxides on the cathode, the deposition process occurs in several steps based on adsorption of metal hydroxyl ions on the deposits Eq. (3-6):



Where M represents Co or Ni atoms.

The  $\text{OH}^-$  ion formed at the end of the reaction favours the formation of  $\text{M}(\text{OH})_{\text{ads}}^+$  and enhances the adsorption of  $\text{MOH}^+$ . The adsorption ability of  $\text{Co}(\text{OH})^+$  was considered to be higher than  $\text{Ni}(\text{OH})^+$  this can cause enriching of binary alloy with less noble metal (Co). Since Cobalt is enriched within the binary Ni-Co deposits, the anomalous phenomenon of nickel-cobalt electroplating can be attributed to the stronger adsorption of  $\text{Co}(\text{OH})^+$  [31].

For Ni-Co coating electrodeposited under (cc) method, The SEM inspection of the cross section shows that the average coating thickness was about  $5 \mu\text{m}$  for 30 min of deposition with a gray shining surface (Fig.7). When continuous electroplating is employed, a reduction of the proton and hydrogen evolution was occurred at the same time as the deposition of metal in two steps Eq. (7):

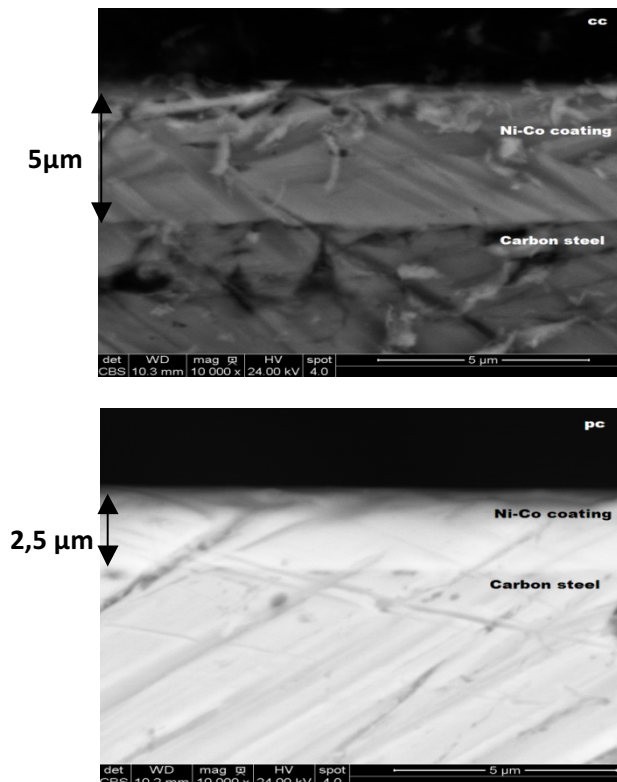


**Fig. 7.** Cross-section micrographs of Ni-Co deposit in continuous (cc) and pulsed (pc) currents on carbon steel substrate after immersion of 30 min in the sulfate media.

The adsorbed species  $\text{Ni(OH)}_{\text{ads}}^+$ ,  $\text{Co(OH)}_{\text{ads}}^+$  and  $\text{H}_{\text{ads}}$  make the electrocrystallization of metal more complicated because they mask the active sites and may, with the metal, forming hydrides or hydroxides which their presence can create overpotential in the interface that will influence the quality of deposits.

However, Ni-Co deposit obtained by (pc) has 2.5  $\mu\text{m}$  of thickness for 30 min of immersion in the plating solution with smooth, uniform and fine grained Ni-Co film without defects caused by hydrogen evolution (Fig. 8 a & b). It perturbed the crystal growth by increasing the number of nucleation sites and consequently a reduction in the grain size occurs. These results reveal the role of (pc) to increase the free energy to form new nuclei which results in a higher nucleation rate and finer grain size [32]. Fenineche et al. [33] reduced grain size of Ni-Co deposits by using (pc) method. Saber et al. [34] successfully produced nanocrystalline zinc deposits by (pc) in the presence of thiourea and polyacrylamide as additives.

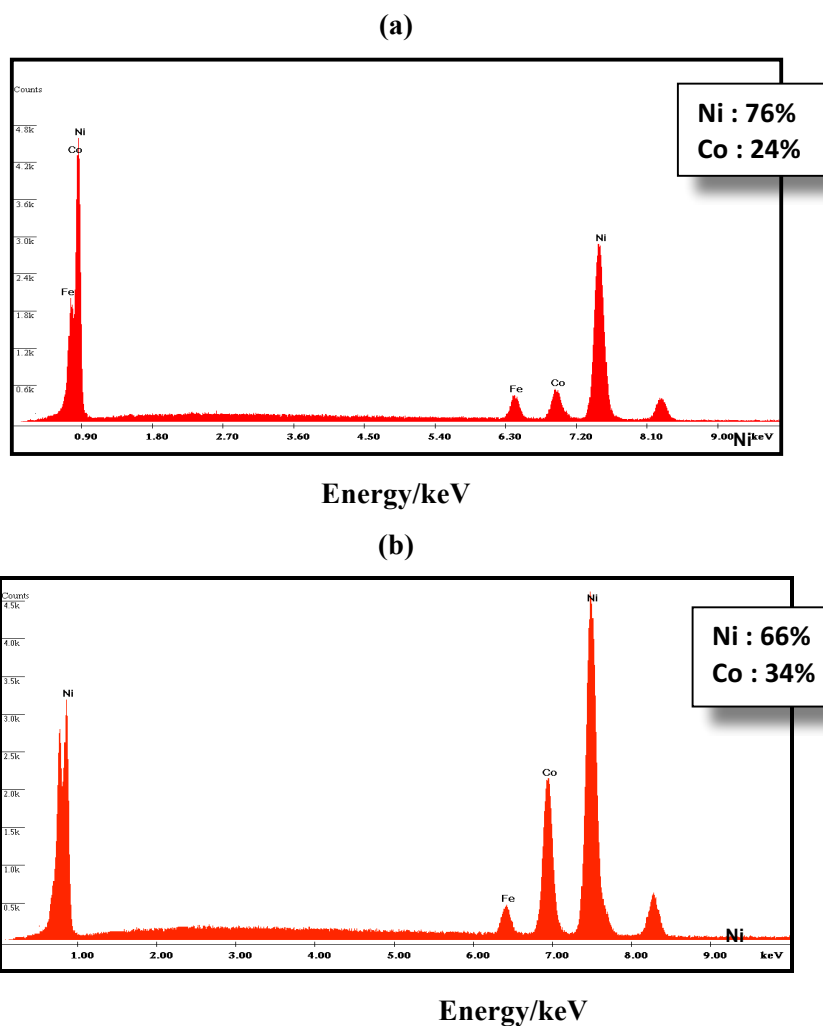


**Fig. 8.** Energy dispersive spectroscopy spectra of Ni–Co deposits R=10 obtained in (a): continuous currents, (b): pulsed currents.

In pulse electrodeposition, high  $I_c$  (cathodic current density) enhances the adatoms population and nucleation rate during  $T_{\text{on}}$ . Pulse currents can affect the electrocrystallization mechanism and controls the physical and mechanical properties of the electrodeposited metal.

The rate of nuclei formation ( $\nu$ ), is given by:

$$\nu = K_1 \exp(-K_2/|\eta|) \quad (8)$$

Where  $K_1$  is proportionality constant,  $K_2$  including  $I_c$  is the amount of energy needed for nucleation and  $\eta$  is the crystallization overpotential. From above equation, it can be inferred that as  $I_c$  increases the overpotential increases, which in turn increases the nucleation rate resulting in finer crystals. In pulse electrodeposition, fine-grained deposition depends upon what happens during  $T_{\text{on}}$ . Current interruption during  $T_{\text{off}}$  encourages re-nucleation due to desorption of impurities [19].

Yundong Li et al. [13] suggested that the reduction in crystal size may be due to the higher overpotential and the accompanying increase in nucleation rate at instantaneously high current density. Crystallization in an electrodeposition process usually involves two steps. The first step is about the discharge of metal ions and the generation of metal atom. There are two scenarios in the second step:

- 1- The incorporation of metal atom into the crystal and crystal growth.
- 2- The formation of new nucleus when the rate of crystal growth may not be sufficient to cater for generation of atom. It has been proved that the critical radius of the surface nucleus is a function of the overpotential: the higher the overpotential, the smaller the nucleus radius and the higher the nucleation rate.

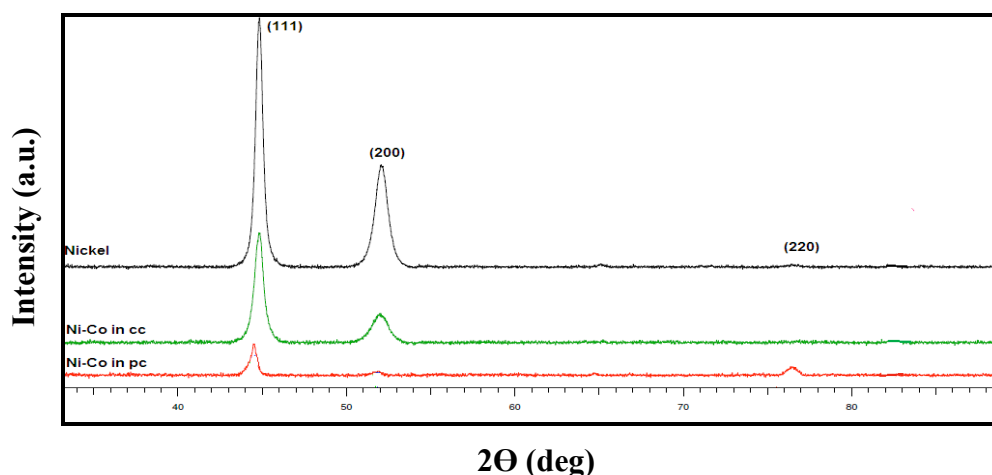
### 3.2.3. XRD analysis

Fig. 9 reveals the XRD patterns of Ni-Co coatings deposited on carbon steel substrate obtained in continuous (cc) and pulsed currents (pc).

In this study, both the continuous and pulsed coatings exhibit single phase of Ni matrix with face-centered cubic (fcc) crystal structure. The fcc peaks are observed in XRD patterns Ni-like structure and peaks corresponding to Co phase (hcp) are not found in the spectra which can be attributed to that the content of cobalt in the (cc) and (pc) coatings is relatively little that it can't be detected. For plain nickel and up to Ni-60 wt.% Co alloys, the structure is found to be fcc with the predominance of (111) orientation.

Under (pc) method, codeposition obviously affects the relative intensity corresponding to different crystal faces, the peak of (200) disappeared and a peak with the orientation (220) was appeared for  $2\theta \approx 76$  deg.

The electrodeposition methods almost have no influence on the position of the diffraction peaks, but the intensity of the diffraction peaks in the pulsed Ni-Co coating is lower, while the peak width of the Ni-Co film obtained by (pc) is broader than that of the Ni-Co alloy coating in (cc). This is attributed to the decrease in the grain size of the Ni-Co electrodeposit under (pc) method, which is proved by the average grain sizes of the coatings calculated from the diffraction peak widths using Scherrer equation Eq. (2) [35]. The Ni-Co coating in (pc) had an average grain size of 6.5 nm, smaller than 8.2 nm that of the Ni-Co alloy coating electrodeposited under continuous method. It has been confirmed by SEM images. The growth of the electrodeposited layer is a competition between the nucleation and crystal growth. Pulsed method provides more nucleation sites and hence retards the crystal growth; subsequently the corresponding Ni-Co coating has a smaller crystal size and texture with finer grains [36, 37].



**Fig. 9.** X-ray diffraction pattern of Ni-Co binary coatings obtained in continuous (cc) and pulsed currents (pc) on carbon steel.

### 3.2.4. Analyze of the metal elements by Glow Discharge Optical Emission Spectroscopy (GDOES)

The thickness of the continuous electrodeposited film (R=10) obtained by GDOES depth profile was approximately about 4  $\mu\text{m}$  close to the value determined with X-ray fluorescence. However, thickness of Ni-Co deposit obtained by (pc) was decreased ( $\sim 2$   $\mu\text{m}$ ). We must clarify that the thickness of film is determined more correctly using cross-section micrographs technique (Fig. 7).

Fig. 10 shows the GDOES depth profile which indicates the percentage of different selected species (nickel, cobalt and iron) which could exist in the deposit.

The distribution of the different metals is disclosed clearly with sharply defined interface between the coating and the cathode [38]. The Glow discharge optical emission spectroscopy (GDOES) is based on the sputtering process and different depths could be eroded. Under (cc) method (Fig. 10a), nickel and cobalt metals are uniformly dispersed inside the deposit and the substrate is appeared after an erosion of a depth about 4  $\mu\text{m}$ .

With using pulsed currents (Fig. 10b), the distribution is not completely uniform. The content of cobalt in the extreme surface is more important than the interior of the deposit, it decreases with erosion and the substrate is reached only after 2  $\mu\text{m}$ , this value is lower than continuous currents. Moreover, the amount of Co in the deposit is increased to 40%, whereas continuous electrodeposited coating presents only about 20%, which is confirmed by XRF analysis.

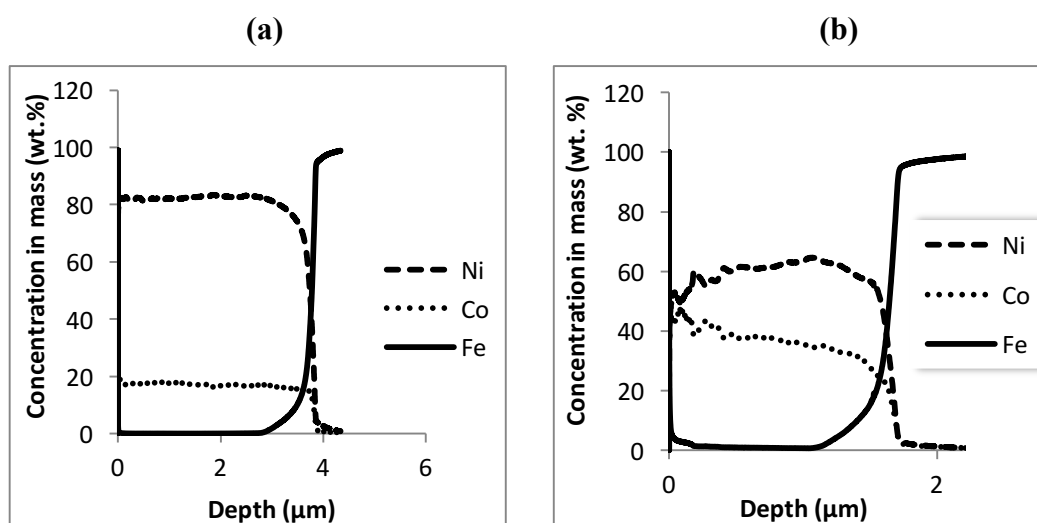


**Fig. 10.** GDOES depth quantified profile of Ni-Co alloy coatings R=10 obtained in (a): continuous and (b): pulsed currents.

### 3.3. Electrochemical behavior comparison of Ni-Co coatings obtained with continuous and pulsed currents in 3% NaCl medium

#### 3.3.1. Open circuit potential (OCP)

Fig. 11 presents the open circuit potential curves against time into 3% NaCl of Ni-Co alloys electrodeposited with (cc) (R=50, 10) and (pc) currents (R=10). Both the Ni-Co alloys in (cc) and in (pc) start with a potential value  $E_{\text{free}} = -450 \text{ mV/SCE}$  and then decrease and stabilize respectively for R=10 (cc), R=10 (pc), R=50 (cc), on  $E_{\text{free}} = -612 \text{ mV/SCE}$ ,  $E_{\text{free}} = -597 \text{ mV/SCE}$  and  $E_{\text{free}} = -550 \text{ mV/SCE}$  (table 4). It seems that this difference in the potential values is due to the percentage of nickel in the deposit; when the potential  $E_{\text{free}}$  increases the nickel content also increases. The curves decrease slowly to attain values higher than those of uncoated steel ( $E_{\text{free}} = -650 \text{ mV/SCE}$ ), showing the galvanic behavior of Ni-Co alloys. It is seen that the potentials of the deposit obtained by pulsed current (R=10) are superior to those obtained by continuous one (R=10 and R=50) for the first 15 min of immersion in 3% NaCl medium, then they decrease and the potentials of R=50 in (cc) become more important.

#### 3.3.2. Surface morphology of Ni-Co alloys after immersion into chloride media

The morphologies of Ni-Co deposits after 1 h and 72h of immersion into 3% NaCl is presented in Fig. 12. When Ni-Co films are electrodeposited under (cc), the initial structure of deposit is destroyed after 1 h of immersion into corrosive solution and cracks and pits are appeared. After 72h, the surface of Ni-Co in (cc) shows that pores number and pits diameter become more important and some deep pores are ed. The formation of pores contributed to hydrogen evolution secondary reaction which due to incorporation of chloride ions in the deposit (Fig. 12b,d). The production of larger pores in chloride media would deteriorate the properties of Ni-Co films, especially the stability. This phenomenon is obviously observed with the atomic ratio R=10 (Fig. 12d).

**Table 4:** Potential  $E_{free}$  recorded from open circuit potential curves in 3% sodium chloride and nickel content in the deposit.

Sample	Ni (wt. %) ( $\pm 0.2$ wt. %)	$E_{free} \pm 5$ (mV/SCE)
Uncoated steel	-	-650
Ni-Co in cc (R=10)	73	-612
Ni-Co in cc (R=50)	91	-550
Ni-Co in pc (R=10)	64	-597

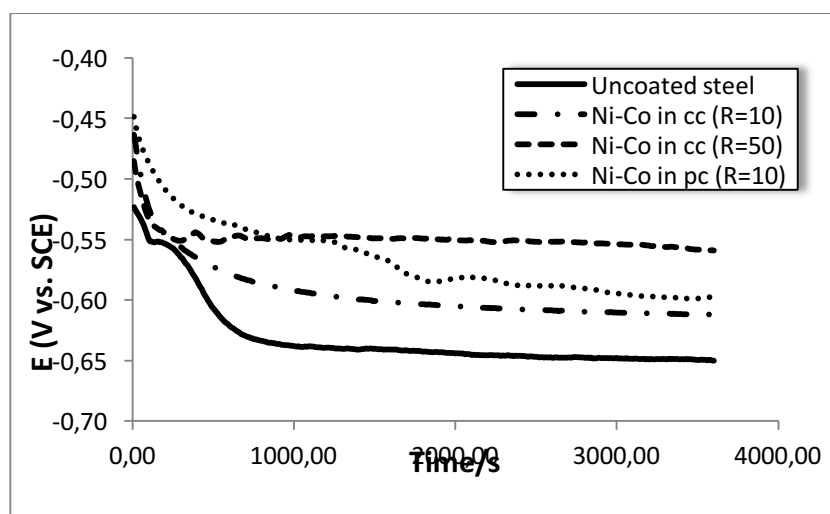


**Fig. 11.** Open circuit potential in 3% sodium chloride of uncoated steel and Ni-Co deposits obtained in continuous and pulsed currents.

When Ni-Co films are electrodeposited under (pc) with a ratio  $R=10$ , granular structure is observed even after 72h of immersion into corrosive solution (Fig. 12f). Ni-Co deposits under (pc) seem to be stronger against chloride ions than those obtained by (cc) with both electrolyte  $R=10$  and  $R=50$  (Fig. 12a,b,c,d). Therefore, cracks and pits can be avoided. It is expected that the Ni-Co films electrodeposited under (pc) will exhibit better physical and chemical properties.

### 3.3.3. Polarization curves

Polarization curves of Ni-Co coatings obtained with (cc) and (pc) are shown in Fig. 13. A cathodic corrosion reaction in a nearly neutral chloride solution for all samples should be the reduction of water at a potential of -1200 mV/SCE [39, 21]:



The cathodic branch includes also the domain of diffusion corresponding to the limit current density of the reduction of dissolved oxygen that starts for uncoated steel at a potential of -900 mV/SCE;



However, the anodic branch corresponds to the dissolution of metals.

The polarization curves of Ni-Co alloys in (cc) and (pc) have the same feature. Only in (pc), there is a shift of the potential to the anodic domain and corrosion current decreases.

For Ni-Co coating obtained in (cc) with Ni/Co atomic ratio ( $R=10$ ), the potentiodynamic plot is shifted towards higher currents when compared to coating obtained in (pc). The cathodic branch of the Ni-Co film with (pc) reveals a Tafel slope corresponding to the reduction of oxygen [33]. The cathodic current of Ni-Co alloy obtained with (pc) is lower than that obtained with (cc) by a factor of 10. The oxidation of the substrate for the case of coated steel with (cc) begins before the oxidation of the (pc) coated steel case, which occurs for more anodic potential value.

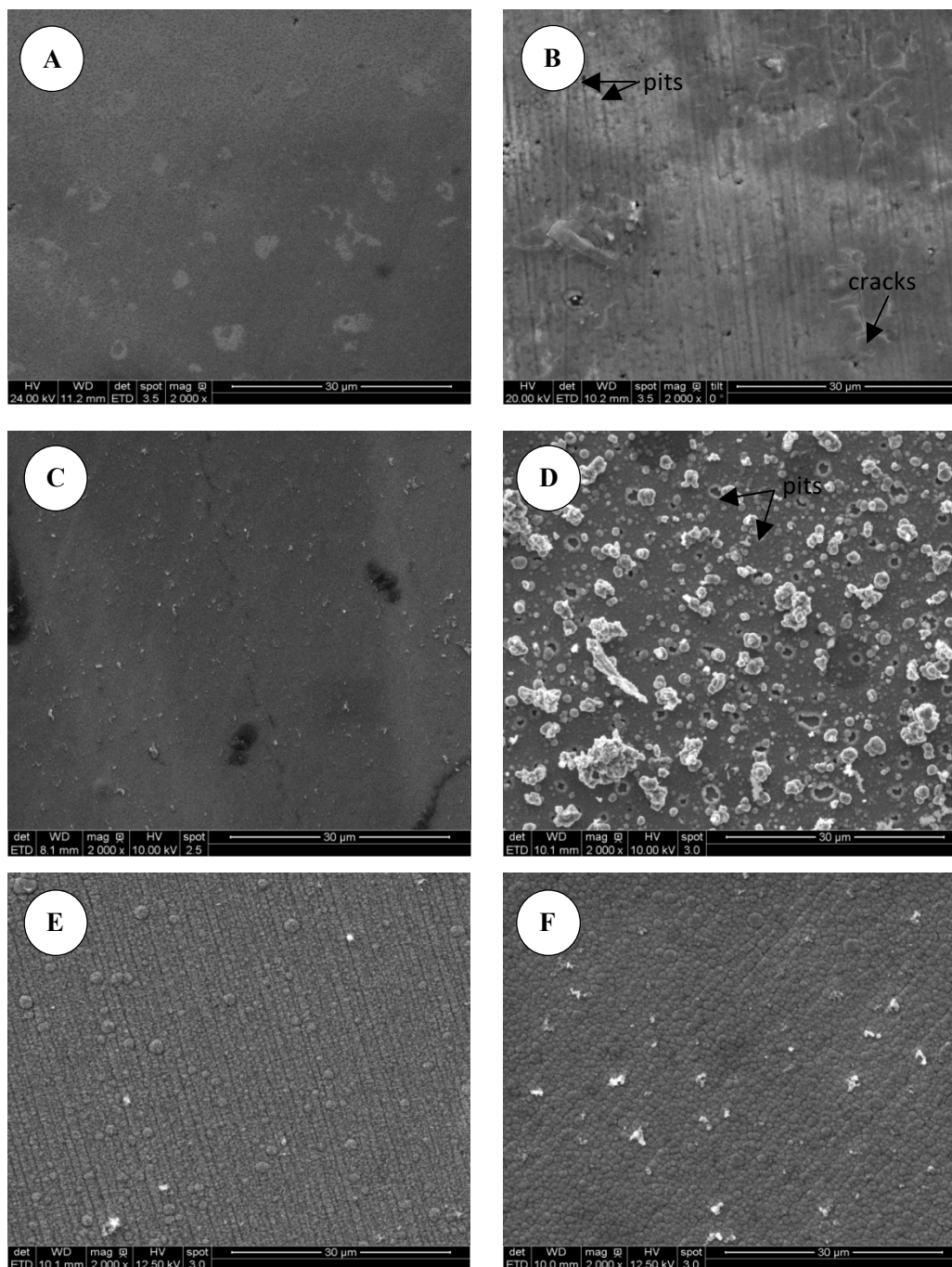


**Fig. 12.** SEM micrographs of Ni-Co coatings: (a) and (b) deposits obtained with R=50 (cc) after 1 h and 72 h of immersion into 3% NaCl, respectively, (c) and (d) R=10 obtained with continuous currents after 1 h and 72 h of immersion into 3% NaCl, respectively, (e) and (f) deposits obtained with R=10 (pc) after 1 h and 72 h of immersion into 3% NaCl, respectively.

The anodic currents of the coated steel sample obtained with (pc) decrease significantly with respect to the coated steel obtained with (cc). Compared to the electrodeposition under (cc), the use of the pulsed electrodeposition process decreases the oxidation rate of carbon steel substrate. According to corrosion potentials and currents, Ni-Co alloy pulsed electrodeposit presents best protection than electrodeposition under (cc) with R=10 due to the high deposit quality obtained by pulse electrodeposition process. In order to achieve the corrosion resistance of Ni-Co alloy coatings electrodeposited in (cc) using a large amount of nickel (R=50), pulsed current was used as alternative approach to reduce bath toxicity with less nickel quantities (R=10).

### 3.3.4. Corrosion parameters

The corrosion parameters such as corrosion potential ( $E_{corr}$ ), corrosion current density ( $i_{corr}$ ), cathodic ( $b_c$ ) and anodic ( $b_a$ ) Tafel slope are calculated by using Tafel fit, Fig. 13, and listed in Table 5.  $E_{corr}$  shifted toward more positive values with a Ni-Co layer obtained in (pc), where  $i_{corr}$  of Ni-Co film electroplated with the pulsed process decreased.

The current density decreases when the Ni-Co coatings were obtained in (pc) which reveals the protective effect of this elaborated film.

**Table 5:** Corrosion parameters extrapolated from polarization curves (Fig.13).

<i>Sample</i>	$E_{corr} \pm 5$ (mV/SCE)	$i_{corr} \pm 10^{-5}$ (mA cm <sup>-2</sup> )	$b_a \pm 0.2$ (mV dec <sup>-1</sup> )	$-b_c \pm 0.2$ (mV dec <sup>-1</sup> )
<b>Uncoated steel</b>	-620	0.29	97	923
<b>Ni-Co in cc (R=10)</b>	-555	0.25	77	430
<b>Ni-Co in cc (R=50)</b>	-399	0.037	88	185
<b>Ni-Co in pc (R=10)</b>	-492	0.0071	65	464

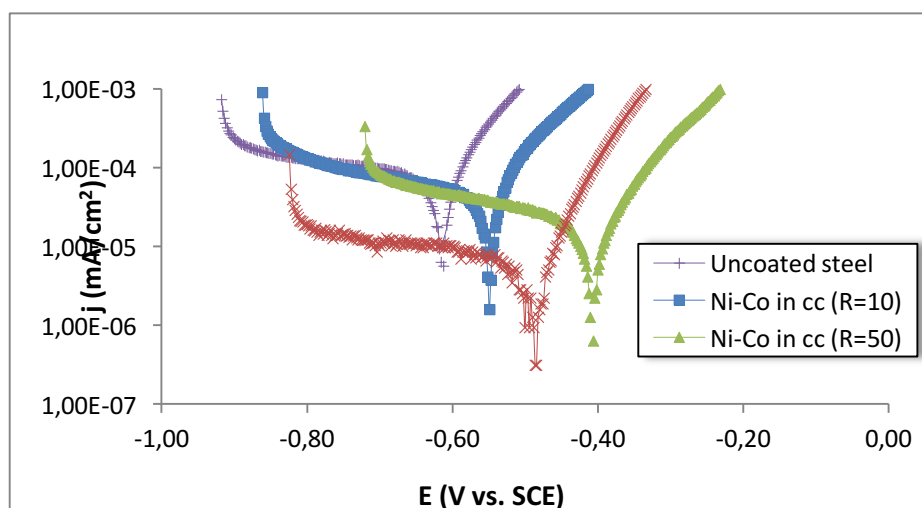


**Fig. 13.** Polarization curves in 3% NaCl solution of nickel, and Ni-Co deposits obtained in continuous and pulsed currents.

## Conclusion

The objective of this work was to study the pulse electrodeposition as alternative method in order to reduce nickel amount in the sulfate plating media and enhance Ni-Co alloys properties compared to deposits obtained by continuous electrodeposition process.

- 1) Ni-Co films obtained with continuous currents present irregular coatings with imperfections caused by hydrogen evolution and grain size of 8 nm, while pulse method can produce Ni-Co coatings with finer crystal grain and smoother surface.
- 2) Both the Ni-Co coatings produced by (cc) and (pc) exhibit single phase of Ni matrix with face-centered cubic (fcc) crystal structure with a decrease in the intensity corresponding to different crystal faces under (pc) method.
- 3) The formed coatings with pulsed currents have better protection and stability against corrosion according to the surface morphology and potentiodynamic results than electrodeposits obtained by continuous currents.
- 4) The improvement of the corrosion properties of the pulsed electrodeposit can be explained by its composition and morphology, which show more refined, compact grains and better hardness coatings unlike the continuous deposits morphology that allow more electrolyte penetration especially with atomic ratio R=10.

**Acknowledgments** -The authors would like to thank the UTINAM Institute, Besançon, France, for their help and access to equipment in the laboratory.

## References

1. Landolt D., *Electrochim. Acta.* 39 (1994) 1075.
2. Duch M., Esteve J., Gomez E., Perez-Castillejos R., Valles E., Micromech J., *Microeng.* 12 (2002) 400.
3. Schlesinger M., Paunovic M., *Modern Electroplating*, Fourth Edition sponsored by the Electrochemical Society, Inc., New Jersey, John Wiley and Sons Publication (2000).
4. William H. Safranek., *The properties of Electrodeposited Metals and Alloys*, A Handbook: Elsevier Publication (1974).
5. Wang G.F., Chan K.C., Zhang K.F., *Scr. Mater.* 54 (2006) 765.
6. Chang L.M., An M.Z., Guo H.F., Shi S.Y., *Appl. Surf. Sci.* 253 (2006) 2132.
7. Wang L.P., Gao Y., Xue Q.J., *Appl. Surf. Sci.* 242 (2005) 326.
8. Qiao G.Y., Jing T.F., Wang N., *Electrochim. Acta.* 51 (2005) 85.
9. Elmen G.W., Franklin J., *Inst.* 206 (1928) 317.
10. Elmen G.W., *Elect. Eng.* 54 (1935) 1292.
11. Golodnitsky D., Rosenberg Yu., Ulus A., *Electrochim. Acta.* 47 (2002) 2707.
12. Kim D., Park D.Y., Yoo B.Y., Sumodjo P.T.A., Myung N.V., *Electrochim. Acta.* 48 (2003) 819.
13. Li Y., Jiang H., Huang W., Tian H., *Appl. Surf. Sci.* 254 (2008) 6865.
14. Lupi C., Dell'Era A., Pasquali M., Imperatori P., *Surf.Coat.Technol.* 205 (2011) 5394.
15. Oskam G., Vereecken P.M., Searson P.C., *J. Electrochem. Soc.* 146 (1999) 1436.
16. Ganesan P., Kumaraguru S.P., Popov B.N., *Surf. Coat. Technol.* 201 (2006) 3658.
17. Pagotto Jr. S.O., *Surf. Coat. Technol.* 122 (1999) 10.
18. Gyftou P., Pavlatou E.A., Spyrellis N., *Appl. Surf. Sci.* 254 (2008) 5910.
19. Chandrasekar M.S., Pushpavanam M., *Electrochim. Acta.* 53 (2008) 3313.
20. Cherkaoui M., Chassaing E., Vu Quang K., *Surf. Coat. Technol.* 34 (1988) 243.
21. Tury B., Lakatos-Varsanyi M., Roy S., *Surf. Coat. Technol.* 200 (2006) 6713.
22. Vazquez-Arenas J., Treeratanaphitak T., Pritzker M., *Electrochim. Acta.* 62 (2012) 63.
23. Vazquez-Arenas J., Pritzker M., *J Solid State Electrochem.* 17 (2013) 419.
24. Gyftou P., Stroumbouli M., Pavlatou E.A., Asimidis P., Spyrellis N., *Electrochem. Acta.* 50 (2005) 4544.
25. Paunovic M., Schlesinger M., mémoire de thèse "Fundamental of electrochemical deposition ", New York (1998).
26. Tian L., Xu J., Xiao S., *Vaccum.* 86 (2011) 27.
27. Malone G.A., Winkelman D.M., *High Performance Alloy Electroforming Final Report*, Report No.8874-927001.
28. Pena-Munoz E., Berçot P., Grosjean A., Rezrazi M., Pagetti J., *Surf. Coat. Technol.* 107 (1998) 85.
29. Kharmachi I., Dhoubi L., Berçot P., Razrazi M., *J. Mater. Environ. Sci.* 6 (2015) 1807.
30. Grigoryan N.S., Kudryavtsev V.N., Zhdan P.A., kolotyркиn I.V., Volynskaya E.A., *Zasch.Met.* 25 (1989) 288.
31. Karslioglu R., Akbulut H., *Appl. Surf. Sci.* 353 (2015) 615.
32. Yang Y., Cheng Y.F., *Surf. Coat. Technol.* 216 (2013) 282.
33. Fenineche N., El Kedim O., Coddet C., *Surf. Coat. Technol.* 48 (1991) 205.
34. Saber K., Koch C.C., Fedkiw P.S., *Mater. Sci. Eng. A.* 341 (2003) 174.
35. Cullity B.D., *Elements of X-ray Diffraction*, 2nd edition, Addison Wesley Publishing, London, 1978.
36. Tury B., Radnoczi G.Z., Radnoczi G., Varsanyi M.L., *Surf. Coat. Technol.* 202 (2007) 331.
37. Boukhouiete A, Creus J., *J. Mater. Environ. Sci.* 6 (2015) 1840.
38. Hammami O., Dhoubi L., Berçot P., Razrazi M., *Surf. Coat. Technol.* 219 (2013) 119.
39. Fan C., Piron D.L., *Electrochim. Acta.* 10 (1996) 1713.

(2016) ; <http://www.jmaterenvironsci.com>